# Oxidation-State and Coordination-Site Specificity Influencing Dimensional Extension and Properties of Two Iron Complexes with Similar Helical Chains

Ying Xu,[a] Lei Han,[a] Zheng-Zhong Lin,[a] Cai-Ping Liu,[a] Da-Qiang Yuan,[a] You-Fu Zhou,[a] and Mao-Chun Hong*[a]

**Keywords:** Iron / Helical chains / Coordination polymer / Oxidation state

Two new iron coordination frameworks, $\{[NH_2(CH_3)_2]_2Fe^{II}(pydc)_2\}_n$ (**1**) and $\{[NH_2(CH_3)_2]Fe^{III}(pydc)_2\}_n$ (**2**) (pydc = 2,5-pyridinedicarboxylate), have been synthesized through the reaction of $FeCl_3$ with $H_2$pydc in dimethylformamide (DMF). **1** crystallizes in an achiral space group $C2/c$, while **2** crystallizes in a chiral space group $P4_32_12$. Both crystal structures consist of $2_1$ helices with similar units: $[Fe^{II}(pydc)_2]^{2-}$ and $[Fe^{III}(pydc)_2]^-$, respectively. The iron oxidation states have been confirmed by means of ESR spectra and bond valence calculations. Quantum chemistry calculations and thermogravimetric analysis have demonstrated their energy and thermal stability. Magnetic studies have revealed that **1** and **2** show weak antiferromagnetic and ferromagnetic interactions between the metal centers, respectively.


## Introduction

Metal-organic coordination networks are the largest class of engineered crystal structures. They expand coordination in diverse dimensions by means of polydentate organic ligands coordinating to metal atoms.[1] Much work has been done towards understanding the molecular packing[2−4] and the relationship between inner structure and collective properties.[5,6] The selection or design of suitable ligands containing certain features, such as functionality and versatile binding modes, plays an important role in determining the topologies and properties of coordination networks.[7−11] Metal atoms, especially their metal oxidation state, also significantly affect the structural extension and properties of coordination networks.[12,13] However, the influence of the metal oxidation state has been comparatively less well investigated.[14,15] Our efforts have focused on constructing coordination networks by assembling multidentate ligand $H_2$pydc and multiple oxidation state iron atoms. Herein, we report the syntheses and characterizations of two new iron coordination frameworks with $2_1$ helical chains: $\{[NH_2(CH_3)_2]_2Fe^{II}(pydc)_2\}_n$ (**1**) and $\{[NH_2(CH_3)_2]Fe^{III}(pydc)_2\}_n$ (**2**), assembled from iron ions and pydc in different coordination modes (Scheme 1).

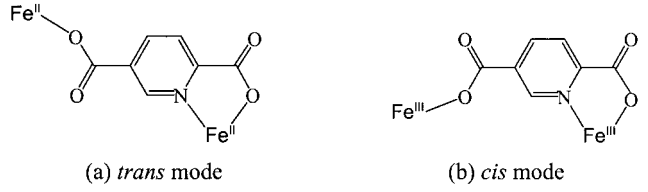


(a) *trans* mode (b) *cis* mode

Scheme 1. Coordination modes of pydc in (a) **1** and (b) **2**

## Results and Discussion

### Syntheses

Although the formation mechanisms are poorly understood, solvothermal synthesis under mild conditions ($T <$ 200 °C, autogenous pressure) is a good way of generating complexes with interesting structures or functional materials, as the nature of organic solvent may drastically effect the formation of compounds.[16−19] In this respect, DMF is a good polar, aprotic solvent with a high boiling point. Consequently, we carried out the solvothermal reaction of iron(III) chloride and $H_2$pydc (1:2 molar ratio) in DMF, which was used to remove the carboxylate group protons and to avoid coordination between the iron atoms and water solvent molecules. Two kinds of well-shaped crystals, dark red blocks for **1** and light yellow dipyramids for **2**, were separated with a moderate yield for **1** and a very low yield for **2**. To obtain a higher yield of **2**, 0.1 mL of $H_2O_2$ (30%) was added to the reaction system, only compound **2** was isolated (44% yield). The formulae of $\{[NH_2(CH_3)_2]_2Fe^{II}(pydc)_2\}_n$ for **1** and $\{[NH_2(CH_3)_2]Fe^{III}(pydc)_2\}_n$ for **2** were revealed by X-ray single-crystal diffraction analy-

[a] State Key Laboratory of Structural Chemistry, Fujian Institute of the Research on the Structure of Matter, Chinese Academy of Sciences,
Fuzhou, Fujian 350002, China
Fax: (internat.) + 86-591-8371-4946
E-mail: hmc@fjirsm.ac.cn

ses and elemental analyses. Clearly, some $Fe^{III}$ was reduced to $Fe^{II}$ as part of a redox reaction. Earlier reports show that the reaction of aromatic N ligands such as pyridine or imidazole derivatives with a transition-metal salt can result in spontaneous metal ion reduction.[20−23] The presence of $[NH_2(CH_3)_2]^+$ in the two compounds results from the decomposition of DMF. No crystals or precipitation were obtained when using *N*,*N*-dimethylacetamide instead of DMF.

## Crystal Structures

### $\{[NH_2(CH_3)_2]_2Fe^{II}(PYDC)_2\}_n$ (1)

Single-crystal X-ray diffraction analysis reveals that complex **1** has a two-dimensional layer structure and crystallizes in a monoclinic space group *C*2/*c*. Figure 1 (a) shows a perspective view of the local coordination environment around the $Fe^{II}$ atom of **1**. The iron atom is hexacoordinate in an $N_2O_4$ environment with a distorted octahedral geometry. Two pyridyl nitrogen donors from different pydc ligands are in an L-shaped arrangement with the central iron atom at the corner; the Fe−N bond length and N(1)−Fe−N(1B) bond angle are 2.170(2) Å and 102.77(14)°, respectively. Four oxygen atoms from different pydc ligands complete its coordination sphere. Fe−O(1) and Fe−O(4A) are 2.098(2) and 2.084(2) Å, respectively. A pydc ligand bridges two $Fe^{II}$ atoms in a *trans* mode through the pyridyl nitrogen atom and an adjacent carboxylate oxygen atom, forming a five-membered chelate ring, while one oxygen atom of the second carboxylate group coordinates another $Fe^{II}$ atom in *trans* position (Scheme 1, a). Thus, an extended two-dimensional layer structure is formed (Figure 2, b) that contains rhombic grids with four $Fe^{II}$ atoms at the corners, with pydc ligands as linkers. The lateral Fe···Fe distances of the $Fe_4$ rhombus are 8.602 Å, the diagonal Fe···Fe distances are 15.066 Å and 8.305 Å.

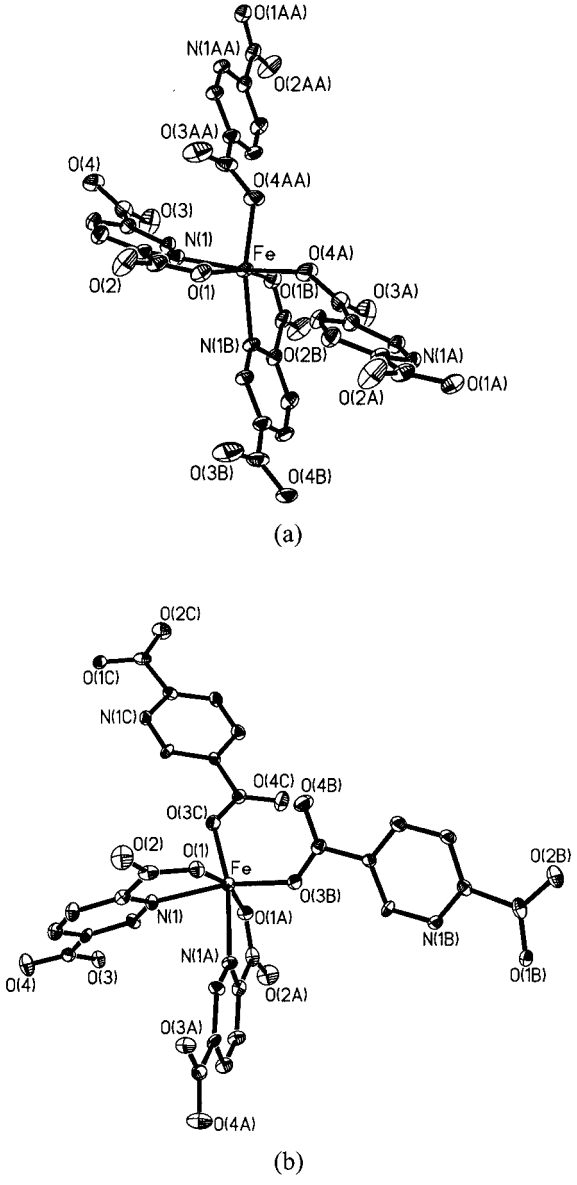


Figure 1. Coordination environments of **1** (a) and **2** (b); ellipsoids are shown at 30% probability

In **1**, the 2D layer $\{[Fe^{II}(pydc)_2]^{2-}\}_n$ can also be considered as arising from $2_1$ helices (Figure 2, a). The helix winds along the *b* axis and the pitch of the helix is the length of *b* (8.305Å). All the helices extend along the same direction, generating a 2D layer structure (Figure 2, b). The layers are parallel to the *ab* plane with a $C_2$ symmetry for neighboring $2_1$ helices. All layers are stacked on top of each other along the *c* axis, with a separation of one half of the *c* length. However, adjacent layers arranged in antiparallel orientation lead to an overall centrosymmetric structure with an achiral space group *C*2/*c* (Figure 2, c). The $[NH_2(CH_3)_2]^+$ cations, omitted in the figures for clarity, lie between the layers to balance charges.

### $\{[NH_2(CH_3)_2]Fe^{III}(PYDC)_2\}_n$ (2)

Single-crystal X-ray diffraction analysis reveals that complex **2** has a three-dimensional structure and crystallizes in the tetragonal chiral space group $P4_32_12$. Figure 1 (b) gives a perspective view of the local coordination environment around the $Fe^{III}$ atom of **2**. As in **1**, the iron atom is hexacoordinate in an $N_2O_4$ environment with a distorted octahedral geometry. Two pyridyl nitrogen donors from different pydc ligands form an L-shaped arrangement with the central iron atom at the corner. The Fe−N(1) bond length and N(1)−Fe−N(1A) bond angle are 2.201(5) Å and 79.8(3)°, respectively. Four oxygen atoms from different pydc ligands complete its coordination sphere. Fe−O(1) and Fe−O(3B) are 1.983(4) and 1.954(4) Å, respectively. Unlike **1**, a pydc ligand bridges two $Fe^{III}$ atoms in a *cis* mode (Scheme 1, b) through the pyridyl nitrogen atom and an adjacent carboxylate oxygen atom, forming a five-membered chelate ring, and one oxygen atom of the second carboxylate group coordinating another $Fe^{III}$ atom on the same side as the chelate ring. Thus, a helical polymer chain is formed that is similar to that in **1** (Figure 2, a; Figure 3, a).

Compound **2** contains $2_1$ helices along the *a* or *b* axis with the pitch being 8.896 Å (Figure 3, a). In contrast to **1**,

  

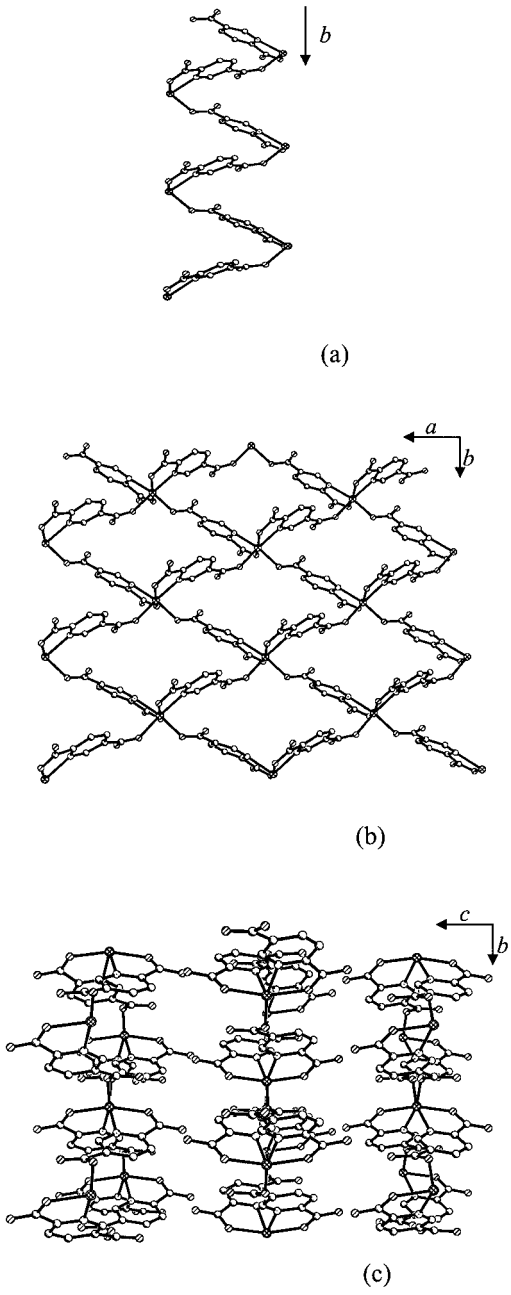


Figure 2. (a) Section of the $2_1$ helical polymer chain along the *b* axis in **1**; (b) 2D layer structure along the *ab* plane in **1**; (c) the stacking 2D layers viewed from the *a* axis in **1**; dimethylamine cations omitted for clarity

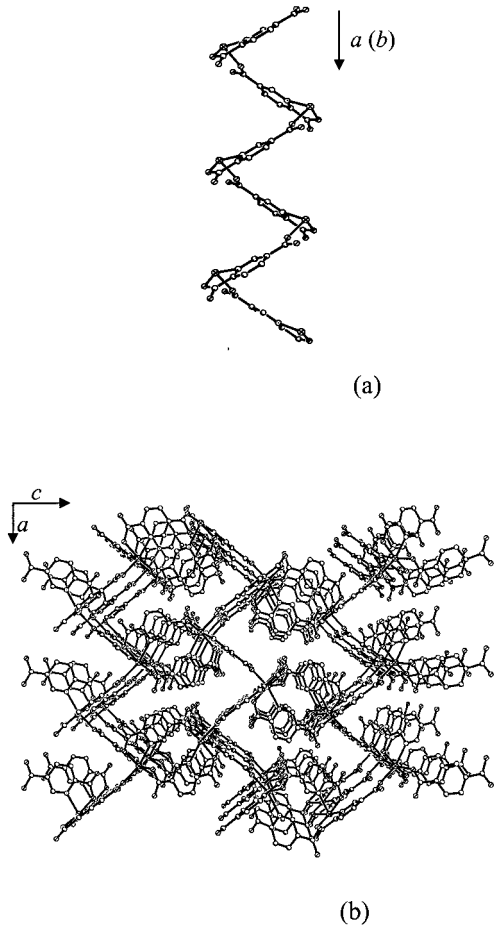


Figure 3. (a) Section of the $2_1$ helical polymer chain along the *a* or *b* axis in **2**; (b) packing diagram of **2** viewed from the *b* axis; dimethylamine cations omitted for clarity

all the helices in **2** are arranged parallel to or perpendicular with the metal atoms as the connective nodes, and so compound **2** has noncentrosymmetry for the overall structure (Figure 3, b). Infinite 3D networks with $4_3$ helices along the *c* axis are formed with the chiral space group $P4_32_12$. $[NH_2(CH_3)_2]^+$ cations lie within the networks to balance charges (omitted from the figures for clarity).

We also found that $Fe^{II}$ atoms coordinated to pydc ligands in a *trans* mode, whereas $Fe^{III}$ atoms coordinated in a *cis* mode, even though both ions underwent the same reaction − the oxidation state of the iron atom might affect the coordination modes of the pydc ligand. Thus, the oxidation state of iron atoms together with the coordination site of pydc ligands specifically influence the dimensional extensions of the two iron compounds. Scheme 2 illustrates the packing, which features two different kinds of inner structures for **1** and **2**.

### Bond Valence Calculation and ESR Spectrum

According to X-ray analyses, element analyses and charge-balance requirements, the bond valence of the Fe atoms in **1** and **2** should be +2 and +3, respectively. This is verified through X-band ESR spectra recorded on polycrystalline samples at room temperature. As expected, **1** is ESR-silent due to non-Kramer spin states ($S = 2$) of the $Fe^{II}$ ion, as a result of either large zero-field splitting or fast relaxation processes.[24] Compound **2** gave a strong, typical response of high-spin $Fe^{III}$ with $g = 3.6615$. Typical low-spin $Fe^{III}$ species have *g* values around 2.[25] Furthermore, bond valence calculations carried out for the $FeN_2O_4$ octahedrons gave bond valence sums (bvs) of +2.39 and +2.92 valence unit (v.u.) for iron atoms in **1** and **2**, respectively. The calculations used reported bond valence parameters for Fe−O and Fe−N bonds.[26] Similar bond valence calcu-

  

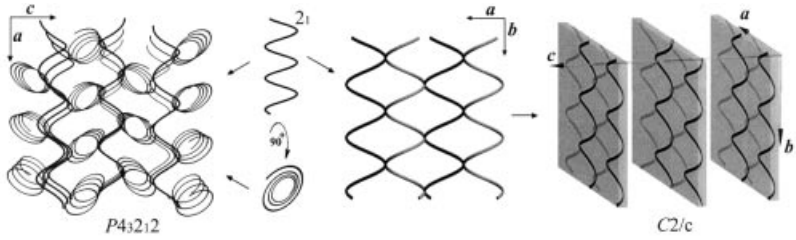


Scheme 2. Arrangement models of $2_1$ helices in complexes **1** and **2**: for **1**, $2_1$ helices along the *b* axis form the 2D layer structure in the *ab* plane, and the adjacent antiparallel layers produce a centrosymmetric achiral space group *C*2/*c*; for **2**, $2_1$ helices along the *a* or *b* axis perpendicular or parallel to each other construct a 3D network with the chiral space group $P4_32_12$

lations have been used successfully for a polyoxovanadate complex.[27]

### Single-Point Energy Calculations and TGA

The organic ligand adopts *trans* and *cis* coordination patterns in **1** and **2**, respectively. Taking account of the energy distinction between the two octahedral coordination units (Figure 1, a, b), single-point energy calculations for them were carried out using the unrestricted Hartree−Fock (UHF) method. For Fe atoms the Los Alamos ECP plus DZ basis set (Lanl2dz)[28] was used, and for C, N, O and H atoms the 6-31G* basis set was employed. Calculations were completed using the Gaussian 98 program.[29] Computational values of −2596.10205193 and −2605.17304136 Hartrees were obtained for **1** and **2**, respectively. These single-point energy calculations show that the energy of the central atom of the octahedral unit in **2** (Figure 1, b) is lower, by ca. 9 Hartrees, than that of the unit in **1** (Figure 1, a), indicating that **2** is thermodynamically slightly more stable than **1**. In agreement, TGA analysis revealed decomposition temperatures of 264 and 315 °C for **1** and **2**, respectively.

### Magnetic Properties

Magnetic measurements were performed for polycrystalline samples of **1** and **2** in the temperature range 270−2 K. For both complexes, as the temperature is lowered to around 35 K, $\chi_M$ increases gradually, and then increases dramatically (Figures 4 and 5). The measured effective magnetic moments $\mu_{eff}$ per iron atom in **1** and **2** are ca. 4.92 $\mu_B$ and 5.80 $\mu_B$, respectively, at 270 K, in agreement with the 4.90 $\mu_B$ for free-ion $Fe^{II}$ in high spin ($S = 2$) and 5.91$\mu_B$ for high-spin $Fe^{III}$ ($S = 5/2$). The results confirm that the oxidation state of iron atoms in **1** and **2** are +2 and +3, respectively.

The magnetic behavior of **1** over the whole temperature range (270−2 K) can be well expressed using Equation (1) derived by Fisher,[30] based on the Hamiltonian $H = -J\Sigma S_iS_{i+1}$ for local spin values $S = 2$, where $J$ is the exchange coupling between two adjacent paramagnetic centers.

$$\chi_M = \{[Ng^2\beta^2S(S+1)]/3kT\}\cdot[(1+u)/(1-u)]$$
$$u = \coth\{[JS(S+1)]/kT\} - kT/[JS(S+1)] \quad (1)$$

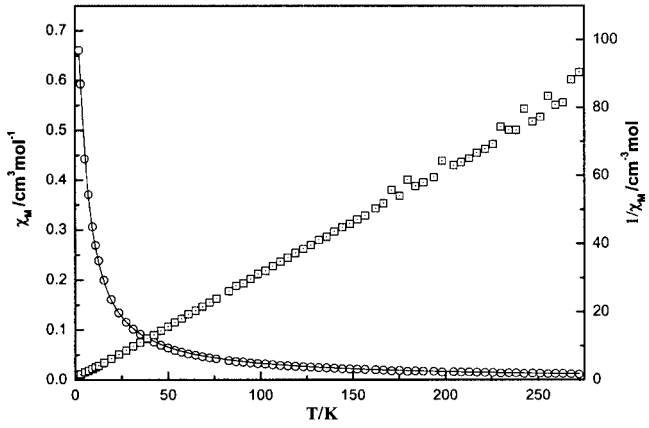


Figure 4. $\chi_M$ vs. $T$ (open circles) and $1/\chi_M$ vs. $T$ (open squares) for **1**; for clarity, only 50% of the recorded data is shown; the line through the symbols (open circles) corresponds to the calculated data of $\chi_M$ for **1** with $g = 2.14$ and $J = -0.36$ cm$^{-1}$

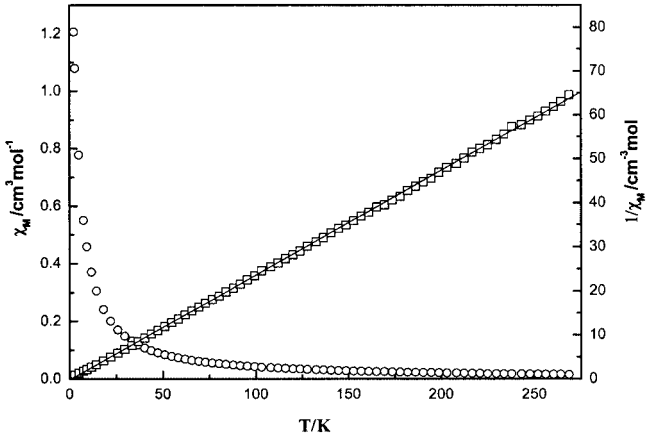


Figure 5. $\chi_M$ vs. $T$ (open circles) and $1/\chi_M$ vs. $T$ (open squares) for **2**; for clarity, only 50% of the recorded data is shown; the line through the symbols (open squares) correspond to the calculated data of $1/\chi_M$ for **2** with calcd. $C = 4.17$ cm$^3$·mol$^{-1}$·K and $T_p = 1.75$ K

For **1**, the best fit parameters are $J = -0.36$ cm$^{-1}$, $g = 2.14$ and $R = 7.66 \times 10^{-6}$, where $R = \Sigma[(\chi_M)_i^{exp} - (\chi_M)_i^{calcd.}]^2/\Sigma[(\chi_M)_i^{exp.}]^2$, illustrating the very weak $Fe^{II}-Fe^{II}$ antiferromagnetic interactions in **1** bridged by pydc ligands. However, the case in **2** is much more complicated, as the network has a three-dimensional extension, and we were

  

unable to model the experimental data. Thus, the $1/\chi_M$ data of **2** was fitted to a Curie−Weiss law [$\chi_M = C/(T - T_P)$], with $C = 4.17$ cm$^3$·mol$^{-1}$·K, $T_p = 1.75$ K and relation factor 0.9997. The small positive Weiss temperature indicates the presence of a weak $Fe^{III}-Fe^{III}$ ferromagnetic interaction, although a detailed elucidation of the magnetic interaction in **2** is awaited.

### Decomposition of DMF

X-ray diffraction analyses revealed the presence of dimethylamine cations $[NH_2(CH_3)_2]^+$ in both **1** and **2**, which result from the decomposition of DMF. IR spectra of **1** and **2** further confirm the presence of $-NH_2^+$ and $-CH_3$ groups. Broad bands in the range of 2700−2250 cm$^{-1}$, together with a weak peak at ca. 2000 cm$^{-1}$, correspond to N−H vibration modes of the $-NH_2^+$ group. In addition, peaks at ca. 2967 and 1460 cm$^{-1}$ indicate C−H stretching and bending modes, respectively, of $-CH_3$ groups. Moreover, elemental analyses are also consistent with the presence of $[NH_2(CH_3)_2]^+$ cations. The decomposition of solvent DMF has been used previously to develop a synthesis of gallium compounds.[19] The product of DMF decomposition could be taken as the unique source of a structure-directing agent for the formation of coordination networks.[19] In fact, dimethylamine, triethylamine, etc. appear to be suitable agents, under solvo(hydro)thermal conditions, to maintain a relatively stable pH and to serve as a mineralizer.[19,31,32−34]

## Conclusion

Two iron complexes with diverse metal oxidation states and coordination patterns of organic ligand have been synthesized by solvothermal reaction. Our focus on the variations in molecular packing, which lead to different dimensional extensions, demonstrates that both the metal oxidation state and the coordination-site of ligands are important in the formation of these compounds.

## Experimental Section

**Materials and Methods:** All reagents and solvents were purchased from commercial sources and used as received. Elemental analyses were determined with an Elementar Vario ELIII elemental analyzer. IR spectra were measured as KBr pellets with a Nicolet Magna 750 FT-IR spectrometer in the range of 200−4000 cm$^{-1}$. ESR spectra were recorded as powder samples at the X-band frequency with a Bruker ER420 spectrometer at room temperature. TGA was recorded with a NETZSCH STA 449C instrument, with samples under nitrogen (15 mL/min), at a heating rate of 15 °C/min. Temperature-dependent magnetic measurements were determined with a Quantum Design SQUID-XL7 magnetometer in an external field of 20 kG.

**Syntheses of Complexes:** Complexes **1** and **2** were obtained from the solvothermal reactions of iron(III) chloride (16.2 mg, 0.1 mmol) and 2,5-pyridinedicarboxylic acid ($C_7H_5NO_4$, 99%, denoted $H_2$pydc) (33.4 mg, 0.2 mmol) in dimethylformamide as solvent ($C_3H_7NO$, 99.8%, denoted DMF) (14 mL). Reactions were performed in Teflon-lined stainless steel Parr bombs (23 mL) under autogenous pressure for 3 d. After cooling the reaction system at a rate of 13 °C/h to 30 °C, dark red crystals (**1**) and light yellow crystals (**2**) were separated, with yields of 36 mg (75%) for **1** and 2 mg (5%) for **2**. To increase the yield of **2**, $H_2O_2$ (30%, 0.1 mL) was added to the system; only compound **2** was obtained, with a higher yield of 19 mg (44%).

**$\{[NH_2(CH_3)_2]_2Fe^{II}(pydc)_2\}_n$ (1):** $C_{18}H_{22}FeN_4O_8$ (478.25): calcd. C 45.21, N 11.72, H 4.64; found C 44.88, N 11.29, H 4.50. IR (KBr pellet, cm$^{-1}$): $\tilde{\nu}$ = 3437 (br., m), 3145 (m), 3029 (m), 2967 (m), 2761 (br., m), 2452 (br., m), 2349 (w), 2000 (w), 1892 (w), 1620(s), 1475 (m), 1455 (m), 1386(s), 1341(s), 1275 (w), 1246 (w), 1165 (w), 1098 (w), 1032 (w), 887 (w), 822 (m), 769 (m), 694 (w), 512 (w). Decomposition temperature: 264 °C.

**$\{[NH_2(CH_3)_2]Fe^{III}(pydc)_2\}_n$ (2):** $C_{16}H_{14}FeN_3O_8$(432.15): calcd. C 44.47, H 3.27, N 9.72; found C 43.82, H 3.39, N 9.68. IR (KBr pellet, cm$^{-1}$): $\tilde{\nu}$ = 3436 (br., m), 3105 (m), 3074 (m), 2960 (m), 2799 (br., m), 2465 (br., w), 2014 (w), 1902 (w), 1778 (w), 1648(s), 1574 (m), 1462 (w), 1391 (m), 1322(s), 1277 (m), 1257 (m), 1233 (m), 1164 (w), 1143 (m), 1117 (w), 1034 (m), 1005 (w), 887 (w), 862 (w), 827 (m), 761 (m), 688 (w), 658 (w), 589 (m), 538 (m), 520 (w). Decomposition temperature: 315 °C.

**X-ray Crystallographic Study:** Crystal data collections were performed at 293 K with a Siemens Smart-CCD diffractometer with graphite-monochromated Mo-$K_\alpha$ radiation ($\lambda$ = 0.71073 Å). Empirical absorption corrections were applied using the SADABS program.[35] Structures were solved with direct methods and refined by full-matrix least squares.[36] Non-hydrogen atoms were refined anisotropically, and the hydrogen atoms were positioned with idealized geometry. All calculations were performed using the SHELXTL program.[37] Crystallographic data and other pertinent

Table 1. Crystal data collection and refinement parameters for $\{[NH_2(CH_3)_2]_2Fe^{II}(pydc)_2\}_n$ (**1**) and $\{[NH_2(CH_3)_2]Fe^{III}(pydc)_2\}_n$ (**2**)

| Complex | **1** | **2** |
|---|---|---|
| Empirical formula | $C_{18}H_{22}FeN_4O_8$ | $C_{16}H_{14}FeN_3O_8$ |
| Formula mass | 478.25 | 432.15 |
| $a$ [Å] | 15.0657(9) | 8.8956(6) |
| $b$ [Å] | 8.3054(5) | 8.8956(6) |
| $c$ [Å] | 17.0198(10) | 21.905(2) |
| β [°] | 100.851(2) | 90 |
| $V$ [Å$^3$] | 2091.6(2) | 1733.4(2) |
| $Z$ | 4 | 4 |
| Crystal system | monoclinic | tetragonal |
| Space group | $C2/c$ | $P4_32_12$ |
| λ [Å] | 0.71073 | 0.71073 |
| ρ [g·cm$^{-3}$] | 1.519 | 1.656 |
| μ [cm$^{-1}$] | 7.74 | 9.23 |
| $T$ [K] | 293(2) | 293(2) |
| Number of data collected | 3048 | 4254 |
| Number of unique data collected | 1836 | 1514 |
| $R_{int}$ | 0.0210 | 0.0851 |
| Data/restraints/parameters | 1836/0/141 | 1514/0/128 |
| $R_1$[a] [$I > 2\sigma(I)$] | 0.0443 | 0.0607 |
| $wR_2$ [a] [$I > 2\sigma(I)$] | 0.1105 | 0.1166 |
| $R_1$ [a] (all data) | 0.0560 | 0.1054 |
| $wR_2$ [a] (all data) | 0.1208 | 0.1342 |
| GOF | 1.036 | 1.157 |
| $\Delta\rho_{min.}$ [e·Å$^{-3}$] | −0.464 | −0.337 |
| $\Delta\rho_{max.}$ [e·Å$^{-3}$] | 0.363 | 0.401 |

[a] $R_1 = \Sigma||F_o| - |F_c||/\Sigma|F_o|$, $wR_2 = [\Sigma w(F_o^2 - F_c^2)^2/\Sigma w(F_o^2)^2]^{1/2}$.

  

Table 2. Selected bond lengths [Å] and angles [°] for **1** and **2**

| Complex **1** | | | |
|---|---|---|---|
| Fe−N(1) | 2.170(2) | Fe−O(1) | 2.098(2) |
| Fe−O(4A) | 2.084(2) | Fe−O(4AA) | 2.084(2) |
| Fe−O(1B) | 2.098(2) | Fe−N(1B) | 2.170(2) |
| O(4AA)−Fe−O(4A) | 87.38(14) | O(4AA)−Fe−O(1B) | 92.27(11) |
| O(4A)−Fe−O(1B) | 99.34(11) | O(4AA)−Fe−O(1) | 99.34(11) |
| O(4A)−Fe−O(1) | 92.27(11) | O(1B)−Fe−O(1) | 163.95(14) |
| O(4AA)−Fe−N(1B) | 165.95(11) | O(4A)−Fe−N(1B) | 86.13(10) |
| O(1B)−Fe−N(1B) | 76.53(9) | O(1)−Fe−N(1B) | 93.36(9) |
| O(4AA)−Fe−N(1) | 86.13(10) | O(4A)−Fe−N(1) | 165.95(11) |
| O(1B)−Fe−N(1) | 93.36(9) | O(1)−Fe−N(1) | 76.53(9) |
| N(1B)−Fe−N(1) | 102.77(14) | | |
| Complex **2** | | | |
| N(1)−Fe | 2.201(5) | O(1)−Fe | 1.983(4) |
| Fe−O(3C) | 1.954(4) | Fe−O(3B) | 1.954(4) |
| Fe−O(1A) | 1.983(4) | Fe−N(1A) | 2.201(5) |
| O(3C)−Fe−O(3B) | 109.2(3) | O(3C)−Fe−O(1) | 96.04(18) |
| O(3B)−Fe−O(1) | 93.24(18) | O(3C)−Fe−O(1A) | 93.24(18) |
| O(3B)−Fe−O(1A) | 96.04(18) | O(1)−Fe−O(1A) | 164.0(3) |
| O(3C)−Fe−N(1A) | 162.95(19) | O(3B)−Fe−N(1A) | 86.16(19) |
| O(1)−Fe−N(1A) | 90.31(19) | O(1A)−Fe−N(1A) | 77.33(19) |
| O(3C)−Fe−N(1) | 86.16(19) | O(3B)−Fe−N(1) | 162.95(19) |
| O(1)−Fe−N(1) | 77.33(19) | O(1A)−Fe−N(1) | 90.31(19) |
| N(1A)−Fe−N(1) | 79.8(3) | | |

Symmetry codes: (A) = $x + 1/2, y - 1/2, z$; (B) = $-x, y, -z + 1/2$; (AA) = $-x - 1/2, y - 1/2, -z + 1/2$ for **1**; (A) = $y, x, -z$; (B) = $-y + 1/2, x + 1/2, z - 1/4$; (C) = $x + 1/2, -y + 1/2, -z + 1/4$ for **2**

information are summarized in Table 1; selected bond lengths and angles for the two complexes are given in Table 2. CCDC-226709 and -226710 contain the supplementary crystallographic data for this paper. These data can be obtained free of charge at www.ccdc.cam.ac.uk/conts/retrieving.html [or from the Cambridge Crystallographic Data Centre, 12 Union Road, Cambridge CB2 1EZ, UK; Fax: (internat.) + 44-1223-336-033; E-mail: deposit@ccdc.cam.ac.uk].

## Acknowledgments

This work was supported by grants from the NNSF of China (No. 20031020) and NSF of Fujian Province. We also thank Professor Song Gao for the magnetism data collection.

[1] D. Braga, *Chem. Commun.* **2003**, 2751−2754.
[2] E. Pidcock, W. D. S. Motherwell, *Chem. Commun.* **2003**, 3028−3029.
[3] J. D. Dunitz, *Chem. Commun.* **2003**, 545−548.
[4] P. A. Maggard, C. L. Stern, K. R. Poeppelmeier, *J. Am. Chem. Soc.* **2001**, *123*, 7742−7743.
[5] O. R. Evans, W. B. Lin, *Acc. Chem. Res.* **2002**, *35*, 511−522.
[6] T. F. Liu, D. Fu, S. Gao, Y. Z. Zhang, H. L. Sun, G. Su, Y. J. Liu, *J. Am. Chem. Soc.* **2003**, *125*, 13976−13977.
[7] S. S.-Y. Chui, S. M.-F. Lo, J. P. H. Charmant, A. G. Orpen, L. D. Williams, *Science.* **1999**, *283*, 1148−1150.
[8] M. C. Hong, Y. J. Zhao, W. P. Su, R. Cao, M. Fujita, Z. Y. Zhou, A. S. C. Chan, *J. Am. Chem. Soc.* **2000**, *122*, 4819−4820.
[9] M. Eddaoudi, J. Kim, N. Rosi, D. Vodak, J. Wachter, M. O'Keeffe, O. M. Yaghi, *Science.* **2002**, *295*, 469−472.
[10] B. F. Abrahams, S. R. Batten, H. Hamit, B. F. Hoskins, R. Robson, *Angew. Chem. Int. Ed. Engl.* **1996**, *35*, 1690−1691.
[11] R. H. Wang, M. C. Hong, D. Q. Yuan, Y. Q. Sun, L. J. Xu, J. H. Luo, R. Cao, A. S. C. Chan, *Eur. J. Inorg. Chem.* **2004**, 37−43.
[12] M.-L. Tong, L.-J. Li, K. Mochizuki, H.-C. Chang, X.-M. Chen, Y. Li, S. Kitagawa, *Chem. Commun.* **2003**, 428−429.
[13] J. Tao, Y. Zhang, M.-L. Tong, X.-M. Chen, T. Yuen, C. L. Lin, X.-Y. Huang, J. Li, *Chem. Commun.* **2002**, 1342−1343.
[14] J. C. Liu, G. C. Guo, J. S. Huang, X. Z. You, *Inorg. Chem.* **2003**, *42*, 235−243.
[15] L. P. Wu, Y. Yamagiwa, I. Ino, K. Sugimoto, T. Kuroda-Sowa, T. Kamikawa, M. Munakata, *Polyhedron* **1999**, *18*, 2047−2053.
[16] D. M. Low, E. K. Brechin, M. Helliwell, T. Mallah, E. Riviere, E. J. L. Mclnnes, *Chem. Commun.* **2003**, 2330−2331.
[17] D. M. Low, L. F. Jones, A. Bell, E. K. Brechin, T. Mallah, E. Rivière, S. J. Teat, E. J. L. Mclnnes, *Angew. Chem. Int. Ed.* **2003**, *42*, 3781−3784.
[18] H. Kominami, J. Kato, S. Murakami, Y. Ishii, M. Kohno, K. Yabutani, T. Yamamoto, Y. Kera, M. Inoue, T. Inui, B. Ohtani, *Catal. Today* **2003**, *84*, 181−189.
[19] C. Paulet, T. Loiseau, G. Férey, *J. Mater. Chem.* **2000**, *10*, 1225−1229.
[20] J. Y. Lu, A. M. Babb, *Inorg. Chem.* **2002**, *41*, 1339−1341.
[21] H. Sugiyama, G. Aharonian, S. Gambarotta, G. P. A. Yap, P. H. M. Budzelaar, *J. Am. Chem. Soc.* **2002**, *124*, 12268−12274.
[22] G. Stupka, L. Gremaud, G. Bernardinelli, A. F. Williams, *Dalton Trans.* **2004**, 407−412.
[23] C.-F. Wang, E.-Q. Gao, H. Zheng, C.-H. Yan, *Chem. Commun.* **2004**, 720−721.
[24] X. S. Tan, J. Chen, Z. N. Chen, P. J. Zheng, W. X. Tang, *Inorg. Chim. Acta* **1995**, *234*, 27−33.
[25] S. J. Lippard, J. M. Berg, *Principles of Bioinorganic Chemistry*, University Science Books, Mill Valley, CA, **1994**.
[26] N. E. Brese, M. O'Keeffe, *Acta Crystallogr., Sect. B* **1991**, *47*, 192−197.
[27] X. Q. Wang, L. M. Liu, G. Zhang, A. J. Jacobson, *Chem. Commun.* **2001**, 2472−2473.
[28] P. J. Hay, W. R. Wadt, *J. Chem. Phys.* **1985**, *82*, 299−310.
[29] M. J. Frisch, G. W. Trucks, H. B. Schlegel, G. E. Scuseria, M. A. Robb, J. R. Cheeseman, V. G. Zakrzewski, J. A. Montgomery, R. E. Stratmann, J. C. Burant, S. Dapprich, J. M. Millam, A. D. Daniels, K. N. Kudin, M. C. Strain, O. Farkas, J. Tomasi, V. Barone, M. Cossi, R. Cammi, B. Mennucci, C. Pomelli, C. Adamo, S. Clifford, J. Ochterski, G. A. Petersson, P. Y. Ayala, Q. Cui, K. Morokuma, D. K. Malick, A. D. Rabuck, K. Raghavachari, J. B. Foresman, J. Cioslowski, J. V. Ortiz, B. B. Stefanov, G. Liu, A. Liashenko, P. Piskorz, I. Komaromi, R. Gomperts, R. L. Martin, D. J. Fox, T. Keith, M. A. Al-Laham, C. Y. Peng, A. Nanayakkara, C. Gonzalez, M. Challacombe, P. M. W. Gill, B. G. Johnson, W. Chen, M. W. Wong, J. L. Andres, M. Head-Gordon, E. S. Replogle, J. A. Pople, Gaussian 98, revision A.5, Gaussian, Inc., Pittsburgh, PA, **1998**.
[30] M. E. Fisher, *Am. J. Phys.* **1964**, *32*, 343−346.
[31] M. H. Zeng, S. Gao, X.-L. Yu, X.-M. Chen, *New J. Chem.* **2003**, *27*, 1599−1602.
[32] R. M. Barrer, *Hydrothermal Chemistry of Zeolites*, Academic Press, London, **1982**.
[33] S.-H. Feng, R.-R. Xu, *Acc. Chem. Res.* **2001**, *34*, 239−247.
[34] Y.-P. Zhang, C. J. O'Connor, A. Clearfield, R. C. Haushalter, *Chem. Mater.* **1996**, *8*, 595−597.
[35] G. M. Sheldrick, *SADABS, Program for Empirical Absorption Correction of Area Detector Data*, University of Göttingen, Germany, **1996**.
[36] G. M. Sheldrick, *SHELXS 97, Program for Crystal Structure Solution*, University of Göttingen, Germany, **1997**.
[37] G. M. Sheldrick, *SHELXTL 97, Program for Crystal Structure Refinement*, University of Göttingen, Germany, **1997**.

Received March 29, 2004
Early View Article
Published Online October 1, 2004

  